Available online at www.sciencedirect.com
ScienceDirect
Journal of Catalysis 244 (2006) 52–64
JOURNAL OF CATALYSIS
www.elsevier.com/locate/jcat

Heterogenized vanadyl cations over modified silica surfaces: A comprehensive understanding toward the structural property and catalytic activity difference over mesoporous and amorphous silica supports

S. Shylesh, A.P. Singh *

Inorganic and Catalysis Division, National Chemical Laboratory, Pune - 411 008, India

Received 24 May 2006; revised 2 August 2006; accepted 3 August 2006

Available online 27 September 2006

Abstract

Using a postsynthesis grafting method, 3-aminopropyltriethoxysilane (3-APTS) was functionalized over silica gel and mesoporous silica materials like SBA-15 and MCM-41. Vanadyl cations were then immobilized over the functionalized amino groups of the silica samples and used as a catalyst in the liquid-phase oxidation reaction of cyclohexane. Elemental analysis, PXRD, TEM, N_2 adsorption–desorption isotherms, FTIR, ^{13}C and ^{29}Si MAS NMR, UV–vis, and EPR techniques were used to characterize the developed materials. Characterization results suggest that the percentage of 3-APTS grafting depends on the number of isolated and geminal silanol sites of the support material, the solvents used during the grafting reactions, and the sample pretreatment conditions. We found that using toluene as the dispersing medium and Si-MCM-41 as a support provides the maximum amount of amine functionalization, and thereby the highest percentage of vanadium immobilization. Catalytic activity and metal leaching studies show that vanadium-immobilized mesoporous solids are more active and stable than the silica gel-functionalized vanadium catalyst and a framework-substituted V-MCM-41 catalyst. The enhanced activity and stability of the immobilized vanadium catalysts compared with the V-MCM-41 and silica gel samples are attributed to the active metal site isolations, as well as to the spatial restrictions imparted from the concave silica surfaces of the mesoporous solids rather than the convex silica surfaces of the silica gel sample.

Keywords: Mesoporous solids; Silica gel; 3-APTS; Vanadium; Oxidation

1. Introduction

Mesoporous silica materials like SBA-15 and MCM-41 with high surface area, uniform pore size, and high thermal stability are of considerable research interest in shape-selective heterogeneous catalysis, adsorption, separation, ion exchange, and hosts for various kinds of molecules [1–5]. The ability to control and to tune the pore size, morphology, and surface silanols has increased their applications dramatically [6,7]. However, a major drawback of these materials lies in their inherent inert nature toward various organic transformations, and hence surface modifications are necessary to make then more suitable, especially in the field of catalysis. Thus, the incorporation of transition metals into the framework of mesoporous materials is a novel technique for introducing active metal sites and thereby extends its applicability in heterogeneous catalysis, where the zeolite catalyst cannot perform [3,4]. However, these framework-substituted materials have serious drawbacks due to their low metal content and lower activity (because many of the active sites are well buried inside the pore channels), and the gradual decrease in catalytic activity after each cycle. Thus, the heterogenization of useful homogeneous catalysts on mesoporous solids is an area of research interest that is expanding due to considerable refinements in synthesis procedures. This technique provides potential advantages over its homogeneous counterparts, including easy separation of the catalyst and enhanced activity [8–12]. In previous work, various metal complexes were occluded inside the pores of the mesoporous support (using, e.g., a “ship in a bottle” technique) or grafted to

* Corresponding author. Fax: +91 2025902497.
E-mail address: ap.singh@ncl.res.in (A.P. Singh).

0021-9517/$ – see front matter
doi:10.1016/j.jcat.2006.08.002

the internal silanol sites; the activity of the catalysts was questionable due to leaching of the confined metal complexes under drastic liquid-phase reaction conditions [13]. However, the immobilization of homogeneous metal catalysts by strong chemical bonding to organo-modified mesoporous materials enhances their potential in two ways, by making them truly heterogeneous and by increasing activity.

Surface modifications over mesoporous materials are generally performed by two common ways: a postsynthesis method and a direct co-condensation method. Compared with postsynthesis grafting methods, which use a two-step synthesis procedure, the direct method allows preparation of nanoporous organic–inorganic hybrid materials in a limited time. However, the resultant materials usually show less structural ordering, and the organosilane precursor must be chosen carefully to avoid phase separations and Si–C bond cleavages during both synthesis and the surfactant removal process. On the other hand, the postsynthesis methods have the following advantages: (i) The structure of the resultant mesoporous materials is ordered after the grafting reactions; (ii) the functional groups can be chosen according to the requirements; and (iii) the obtained materials show higher hydrothermal stability. Even though the literature displays a wide spectrum of organo-tethered mesoporous materials with active functionalities, thiol (–SH) and amine ($–NH_2$) terminated mesoporous materials receive more attention than the other active pendant groups (–Cl, –OH, $(–PPh_3)_3$) for the immobilization of various traditionally used active homogeneous catalysts [5,6,9]. Recently, we demonstrated the immobilization of $(VO)^{2+}$ on an amino-terminated organosilane MCM-41, considering the point that harder transition metal ions form stable complexes with ligands with harder donor sites. Characterization of the fresh and spent catalyst after the naphthalene oxidation reaction showed that this significantly affects the structural and morphological features of the MCM-41 support [14]. Consequently, an attempt was made to extend the same procedures over the large-pore hexagonally ordered SBA-15 and on a silica gel sample to gain better insight into the changes occurring on the surface during the silylation process and to facilitate the design of a specific support for grafting and subsequent complexation procedures.

The present paper deals with the immobilization of $(VO)^{2+}$ species on an amino propyl-modified SBA-15/MCM-41/silica gel sample. Although the literature contains several reports over amine-functionalized mesoporous materials, a proper comparison or a comprehensive understanding of the structural changes and the binding nature of aminopropyl groups over SBA-15, MCM-41, and silica gel surfaces during postsynthesis modifications is highly limited. Thus, this work probes in detail the affect of solvents used for grafting of the aminopropyl groups, the effect of amino groups anchored toward the structural stability of the mesoporous silicas and the nature of vanadium species formed over SBA-15/MCM-41/silica gel surfaces. The obtained materials are then used as catalyst in the liquid-phase oxidation of cyclohexane using aqueous H_2O_2 as an oxidant and were compared with a hydrothermally synthesized V-MCM-41 sample.

2. Experimental

2.1. Materials

The following reagents were used for the synthesis of pristine SBA-15, MCM-41, and organo-modified mesoporous materials: tetraethyl orthosilicate (TEOS, Aldrich), silica gel (Loba Chemie, $S_{BET} = 444\ m^2\,g^{-1}$), pluronic 123 (P123, BASF), cetyl trimethyl ammonium bromide (CTMABr, Aldrich), 3-aminopropyltriethoxysilane (3-APTS, Lancanster) and vanadyl sulphate ($VOSO_4{\cdot}3H_2O$, Aldrich). All chemicals were used as received.

2.1.1. Synthesis of siliceous mesoporous materials (Si-SBA-15 and Si-MCM-41)

Siliceous SBA-15 was synthesized according to the procedure reported by Zhao et al. [2]. In a typical synthesis procedure, 2 g of P123 surfactant was stirred with 20 ml of deionized water at 35 °C. The mixture was stirred until the surfactant gets dissolved, followed by the addition of 30 g of 2 M HCl solution. The stirring was allowed to run for another 30 min, after which 4.5 g of TEOS was added dropwise to the stirred solution mixture. The mixture was then stirred for 24 h at 35 °C, transferred in an autoclave, and heated for another 48 h at 100 °C. The solid material obtained was then filtered, washed with water (5 times), and calcined at 540 °C for 6 h at a heating ramp of 1 °C/min to remove the occluded polymeric surfactants.

Gel with a molar composition of SiO_2:0.39 Na_2O:0.48 CTMABr:0.29 H_2SO_4:100 H_2O was used for the synthesis of siliceous MCM-41 [14]. The gel mixture was stirred for 2 h under ambient conditions and finally transferred into a Teflon-lined autoclave and kept at 100 °C for 72 h. The solid material thus obtained was then filtered, washed well with copious amounts of water until the filtrate showed a neutral pH, then air-dried. The surfactant inside the pores of the mesoporous material was removed by calcination as described above.

2.1.2. Functionalization of 3-aminopropyltriethoxysilane over mesoporous silica/silica gel (NH_2-SBA-15/ NH_2-MCM-41/NH_2-SG)

Before functionalization, the support silica materials were dehydrated at 150 °C for 3 h to remove the physisorbed water molecules. Postsynthesis modification of the mesoporous material was done by refluxing 1 g of the silica sample with 2.2 mmol of 3-aminopropyltriethoxysilane in 50 ml of dry toluene. The mixture was then allowed to run for 6 h at 100 °C. Finally, the material was filtered, washed with toluene, Soxhlet-extracted using a mixture of diethyl ether (100 ml) and dichloromethane (100 ml) for 24 h. and dried under vacuum. To evaluate the influence of solvents during grafting reactions, the grafting process was repeated using such solvents as dichloromethane, acetone, and chloroform.

2.1.3. Immobilization of $(VO)^{2+}$ cations over amino-terminated mesoporous silica/silica gel (VO–NH_2-SBA-15/VO-NH_2-MCM-41/VO-NH_2-SG)

Vanadyl cations were immobilized over aminopropyl-modified silica materials by treating NH_2-SBA-15/NH_2-MCM-41/NH_2-silica gel samples with an alcoholic solution of vanadyl sulphate. Typically, 1 g of organo amine-functionalized silica was stirred with a 0.01 M alcoholic solution of vanadyl sulfate for 6 h at 60 °C under nitrogen atmosphere. The process was repeated twice for a maximum coordination of vanadyl groups on the amine-functionalized silica samples. Finally, the pale green-colored mixture was filtered, washed with copious amounts of ethanol and then Soxhlet-extracted with ethanol for 12 h to remove any unanchored vanadyl species. For comparison, the same procedure was repeated on nonmodified SBA-15/MCM-41/silica gel materials to evaluate the role of amino groups in the anchoring of vanadium species. Furthermore, a V-MCM-41 sample was also synthesized hydrothermally. The details of the synthesis procedures have been reported elsewhere [14].

2.2. Characterization

The loading of aminopropyl groups was calculated from the nitrogen content by elemental analysis using an EA1108 Elemental Analyzer (Carlo Erba Instruments). Powder X-ray diffraction (PXRD) patterns of SBA-15 samples were collected on a Siemens D5005 diffractometer using CuK_α ($\lambda = 1.5404$ Å) radiation. The diffractograms were recorded in the 2θ range of 0.5°–5° with a step size of 0.01° and a step time of 10 s. PXRD patterns of MCM-41 samples were recorded on a Rigaku D MAX III VC instrument using Ni-filtered CuK_α radiation at 1.5°–10° (2θ), with a scanning rate of 1°/min. TEM analysis of the mesoporous samples were performed on a JEOL-JEM-1200 EX instrument at an accelerated voltage of 100 kV. The specific surface area, total pore volume, and average pore diameter were measured by an N_2 adsorption–desorption method using NOVA 1200 (Quanta Chrome) instrument. The samples were activated at 200 °C for 3 h under vacuum, after which adsorption–desorption was done by passing nitrogen over the sample, which was kept under liquid nitrogen. Pore size distribution (PSD) was obtained from the adsorption branch of the isotherm using the Barret–Joyner–Halenda (BJH) method.

FTIR spectra of the solid samples were taken in the range of 4000–400 cm^{-1} on a Shimadzu FTIR 8201 instrument. Before analysis, the samples were flushed in nitrogen atmosphere at 100 °C for 3 h, and the spectra were acquired at 4 cm^{-1} resolution and averaged over 48 scans. Proton-decoupled solid-state ^{13}C and ^{29}Si MAS NMR spectra were recorded on a Bruker MSL 300 NMR spectrometer with a resonance frequency of 75.5 MHz for ^{13}C and 59.9 MHz for ^{29}Si, using glycine and TMS as reference. The resolution obtained in the ^{29}Si NMR spectra is sufficient for accurate peak assignments, and the relative peak area of each site was obtained from the curve-fitting analysis, using a series of Gaussian curves. Diffuse-reflectance UV–vis spectra were recorded in the range of 200–800 nm with a Shimadzu UV-2101 PC spectrometer, using $BaSO_4$ as reference. Samples were repeatedly flushed in nitrogen atmosphere at 100 °C for 6 h before recording the spectra. EPR spectra of the solid samples were recorded at room temperature conditions operating at X-band frequency on a Bruker EMX spectrometer.

2.3. Catalytic reaction

Oxidation reactions were performed in a round-bottomed flask fitted with a water-cooled condenser, using 30 wt% aqueous H_2O_2 as an oxidant. The reactant mixtures of cyclohexane (0.8 g, 10 mmol), oxidant (1.12 g, 10 mmol), and acetonitrile solvent (5 ml) were added to 0.1 g of catalyst and heated at a constant temperature (80 °C) under magnetic stirring (ca. 800 rpm). After reactions, the reaction mixture was cooled to room conditions, and the catalyst was separated from the reaction mixture by centrifugation. The oxidized products were analyzed on a gas chromatograph (HP 6890) equipped with a flame ionization detector (FID) and a capillary column (5-μm cross-linked methyl silicone gum, 0.2 mm × 50 m), and the products were further confirmed by authentic samples.

3. Results and discussion

3.1. Structural characterization

In the present study, postsynthesis grafting methods were used for the functionalization of aminopropyl groups, because it is known that the co-condensation of TEOS and 3-APTS groups can cause severe damage to the mesopore structural ordering in an acidic route (SBA-15 synthesis) compared with the basic synthesis as performed over MCM-41 [15]. The aminopropyl groups introduced in an acidic media are easily protonated and may disorder the mesopore structure in the direct synthesis of NH_2-SBA materials. In addition, the disordering also may arise due to the following reasons: (i) formation of zwitterions due to the interaction of the amine and silanol groups, preventing the interaction of the oligomerized silicates with the surfactants; (ii) interaction of the amine groups with the hydrophilic ethylene oxide (EO) groups of the surfactant chain, and repulsion between the hydrophilic tail groups of the amino propyl and the hydrophobic propylene oxide (PO) groups of the block copolymer groups; and (iii) cross-linking of the ammonium groups with the silanols and the variation in the pH of the gel mixture [15–17]. Because of these factors, we believe that postsynthesis modifications are more suitable for comparing the structural changes occurring during the anchoring of the 3-APTS groups, because they provide more insight into the physical properties of the support surfaces than the complicated gel chemistry arising from the direct synthesis method.

Toluene was the dispersing medium used in the functionalization of 3-APTS over mesoporous and silica gel supports. Nitrogen elemental analysis showed that the percentage of amine loading varied in the order MCM-41 > Silica gel > SBA-15, corresponding to ∼76%, ∼70%, and ∼66%, respectively, used for functionalization. Because the same amount of 3-APTS was added over the three support materials, the observed discrepancies in the percentage of amine loading arise from the differ-

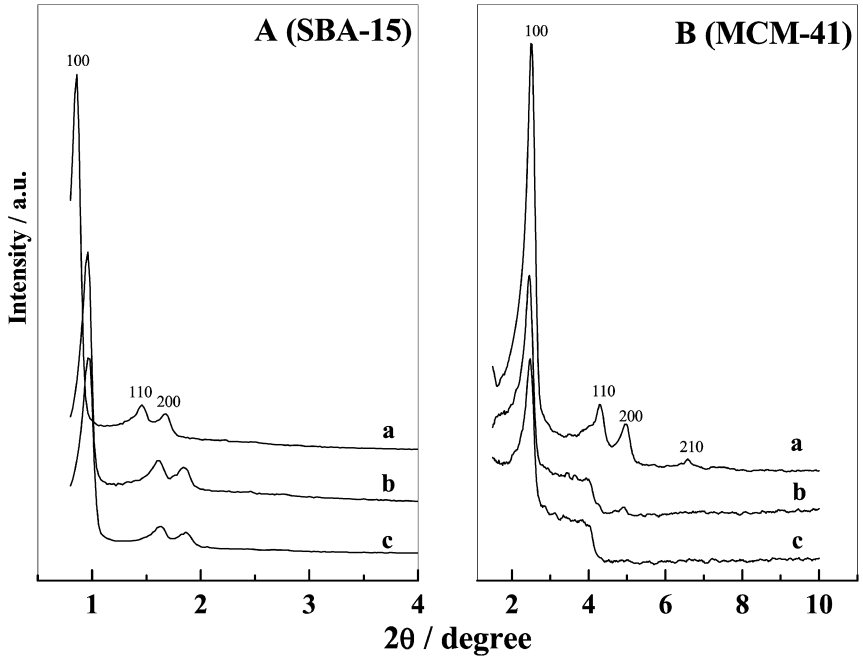

Fig. 1. XRD patterns of (A) SBA-15 samples and (B) MCM-41 samples, where (a) calcined sample, (b) aminopropyl modified sample and (c) vanadium-immobilized sample.

ence in the number and nature of silanol/siloxane bonds on the support surface. Thus, to probe whether the solvents used had any effect on the percentage of 3-APTS functionalization compared with toluene, the grafting procedures were extended using such solvents as dichloromethane, acetone, and chloroform over MCM-41. We found that after 6 h, the percentage of amine loading varied in the following order: toluene (∼76%), chloroform (∼70%), acetone (∼63%), and dichloromethane (∼59%). Thus, among the solvents evaluated, toluene showed the best level of amine functionalization, with a percentage loading >70%. In addition, XRD patterns also show that the structural ordering of the resultant functionalized mesoporous materials (NH_2-MCM-41) also differs according to the nature of the solvent used (figure not shown). Thus, dichloromethane-refluxed mesoporous MCM-41 sample keeps the structural ordering intact, whereas the sample refluxed in toluene exhibited the lowest structural ordering. A comparison of this result with the elemental analysis data suggests that the improved mesoporous structure obtained in low boiling solvents relates to the decrease in the percentage of aminopropyl loadings. These results emphasize the importance of solvents used for organo functionalization studies and suggest that if the goal is to increase the percentage of amine groups, toluene as solvent gives the best results, whereas mesopore structural features are retained over low-boiling solvents, which have fewer functionalized organic groups. The percentage of vanadium immobilized over the 3-APTS functionalized samples, estimated by ICP analysis, is close to that over the NH_2-MCM-41, NH_2-silica gel, and NH_2-SBA-15 samples (Table 3). Meanwhile, the samples prepared without using a 3-APTS spacer show the absence of vanadium, highlighting the role of amino groups in stabilizing the vanadium complexes (see Section 2).

The small-angle X-ray diffraction (XRD) patterns of SBA-15, NH_2-SBA-15, and $(VO)^{2+}$ cations immobilized SBA-15 samples are given in Fig. 1A, with the corresponding MCM-41 samples given in Fig. 1B. The XRD pattern of pristine SBA-15 shows three (*hkl*) reflections of (100), (110) and (200) in the 2θ range of 0.8°–2° indexed to two-dimensional (2D) hexagonal *p6mm* symmetry, indicating a highly ordered hexagonal structure [2]. In the same way, the pristine MCM-41 solid sample shows four Bragg reflexes with hkl reflections of (100), (110), (200), and (210) for a highly ordered hexagonal symmetry. After silylation, the width of the d_{100} peak of both mesoporous materials narrows, possibly related to the homogeneous distribution of the pore structure brought about by the attachment of aminopropyl groups inside the mesopore channels. However, the decrease in intensity of the d_{100} peak after postsynthesis modifications demonstrates the partial structural collapse of the mesoporous materials or the flexibility induced in the silica framework due to the strain generated from the functionalized groups [12]. Comparing the XRD patterns of the two mesoporous materials after modifications shows that the long-range-ordered d_{100}, d_{200}, and d_{210} peaks disappeared in MCM-41, whereas the structural features of SBA-15 features remained intact even after vanadyl cation immobilization. These results show more pronounced structural disordering over MCM-41 compared with over the SBA-15 solids. Evidence that the highly ordered structural features are better preserved over SBA-15 samples than MCM-41 samples after silylation reactions and subsequent metal immobilization is directly provided from the transmission electron microscopy (TEM) images (Fig. 2). TEM of pristine mesoporous SBA-15 and MCM-41 samples shows the images of channels and framework when the electron beam is passed perpendicular to the pore, demonstrating a highly ordered pore structure. Af-

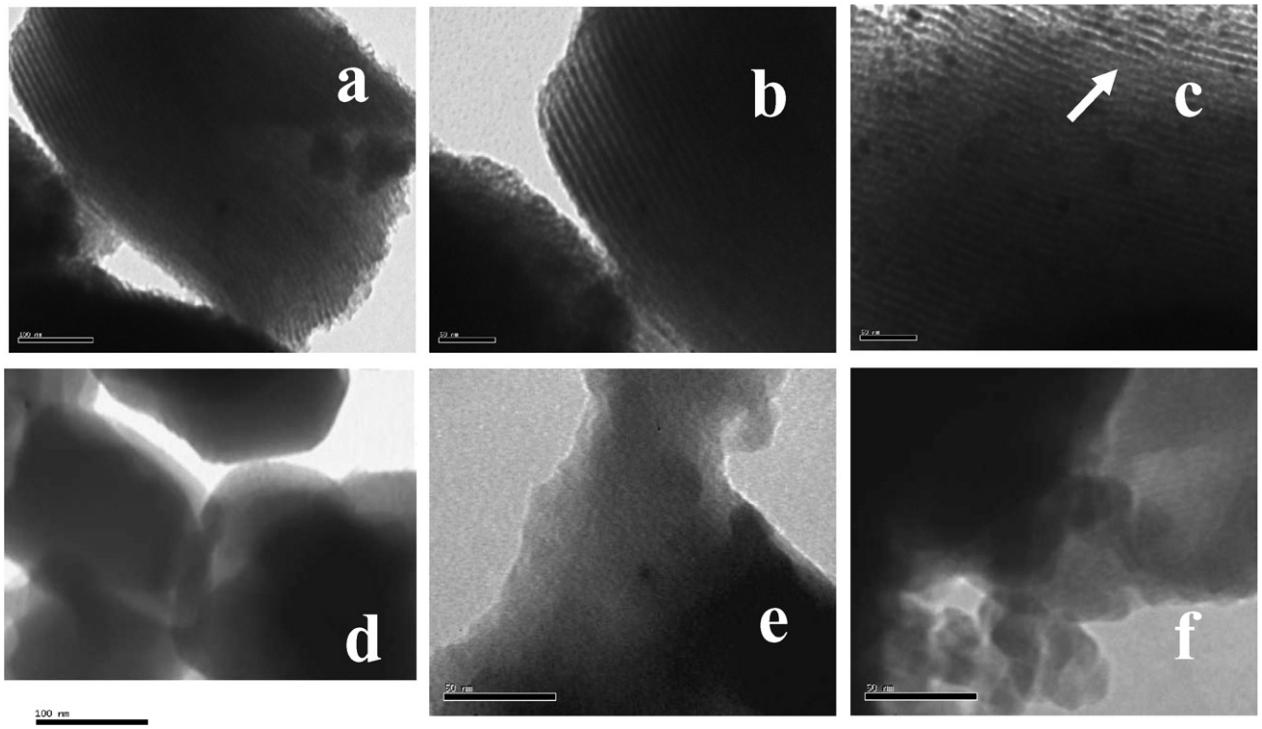

Fig. 2. Transmission electron micrographs (TEM) of (a) Si-SBA-15, (b) NH_2-SBA-15, (c) VO–NH_2-SBA-15, (d) Si-MCM-41 (e) NH_2-MCM-41 and (f) VO–NH_2-MCM-41.

ter silylation, the hexagonal arrangement of SBA-15 is preserved, and after $(VO)^{2+}$ cation immobilization, distinct spots of nanosized metal sites in the ordered mesopore channels can be clearly seen. However, for MCM-41, a significant decrease in the channel ordering was observed after silylation, and the structural degradation became more pronounced after vanadium immobilization, as demonstrated by the XRD patterns. In fact, such results are commonly observed during modifications of MCM-41 and its difference from SBA-15 points to the inherent property between these two mesoporous materials, for example, the difference in hydrothermal stability. Because the pore wall thickness of MCM-41 (1–1.5 nm) is lower than that of SBA-15 (3–6 nm), it is reasonable to assume that the high-temperature organo functionalization and subsequent synthesis procedures can cause some dissociation in the silica framework of MCM-41 and thus account for the partial structural collapse of the material after modifications. Hence, based on the XRD patterns and TEM images, it seems that for postsynthesis modifications, the well-ordered, hydrothermally stable SBA-15 is a matter of choice by comparing the degree of structural collapse of the hexagonal phase during organo functionalization and the subsequent coordination/complexation of metal ions in SBA-15/MCM-41 supports.

The specific surface area of SBA-15, MCM-41, and silica gel was observed at 810, 849, and 444 $m^2\,g^{-1}$ and the textural properties of all samples are summarized in Table 1. The reduction in surface area after amino propyl modification is ∼31% for SBA-15, ∼40% for MCM-41, and ∼37% for silica gel. The decrease in surface area for the modified mesoporous materials shows the anchoring of 3-APTS inside the mesopore channels with subsequent significant reduction of its textural qualities. However, the reduction in surface area is rather less pronounced after immobilization of the vanadyl cations. Nitrogen adsorption–desorption isotherms of calcined, aminopropyl-modified, and vanadyl cations in immobilized SBA-15 and MCM-41 samples are shown in Fig. 3. Both mesoporous solids show type IV isotherms, according to the IUPAC classification. The SBA-15 samples exhibit a sharp increase in N_2 adsorption at a higher P/P_0 value (∼0.7) and a distinct hysteresis loop with an almost parallel adsorption and desorption (type H1). The increased sharpness in the N_2 condensation step points to the uniformity of the mesopore structure [2]. More-

Table 1
Textural characteristics of vanadium-containing mesoporous materials and silica gel

Sample	a_0[a] (nm)	S_{BET} ($m^2\,g^{-1}$)	V_p[b] ($cc\,g^{-1}$)	D_p[c] (nm)	ω_t[d] (nm)
SBA-15	11.4	810	0.93	7.2	4.2
NH_2-SBA-15	10.7	559	0.82	6.7	4.0
VO–NH_2-SBA-15	10.4	532	0.78	6.7	3.7
MCM-41	4.0	849	0.68	3.2	0.8
NH_2-MCM-41	4.2	505	0.61	2.4	1.8
VO–NH_2-MCM-41	4.1	320	0.58	2.8	1.3
SG	–	444	n.d.[e]	n.d.	–
NH_2-SG	–	279	n.d.	n.d.	–
VO–NH_2-SG	–	240	n.d.	n.d.	–
V–MCM-41	4.1	852	0.61	2.5	1.6

[a] $a_0 = 2d_{100}/\sqrt{3}$.
[b] V_p = pore volume.
[c] D_p = pore diameter.
[d] ω_t = Wall thickness = $a_0 - D_p$.
[e] n.d. = not determined.

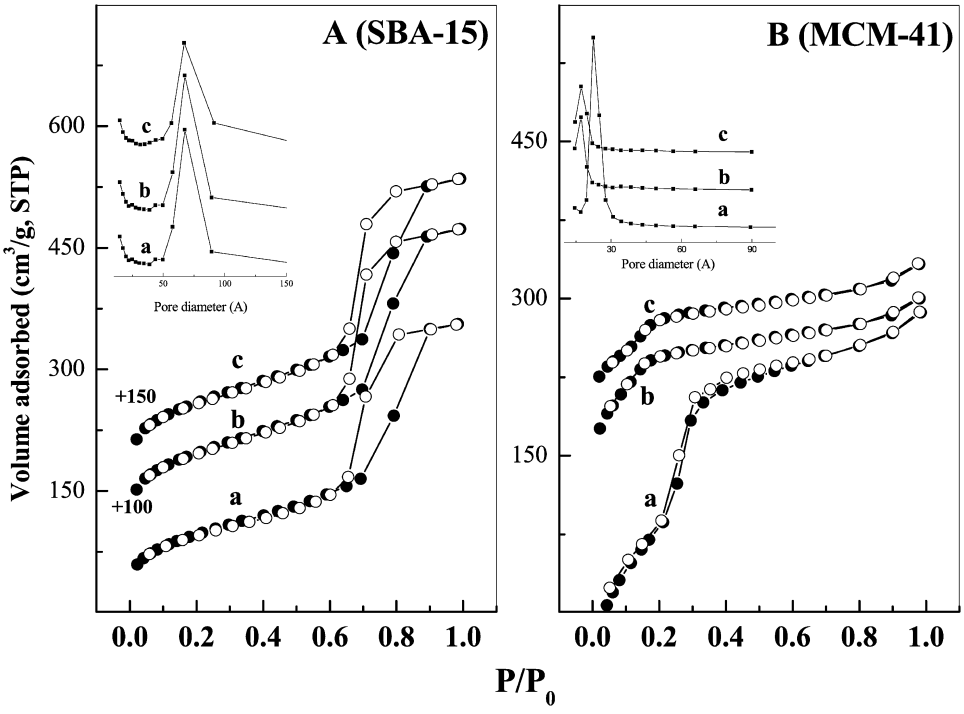

Fig. 3. Nitrogen adsorption–desorption isotherms and pore size distribution profiles (inset) of (A) SBA-15 and (B) MCM-41, where (a) calcined sample, (b) aminopropyl modified sample and (c) vanadium-immobilized sample.

over, the width of the hysteresis loop did not change significantly after aminopropyl functionalization and vanadyl cation immobilization showing the preservation of pore arrangement after the modifications. The N_2 isotherm of MCM-41 displays no hysteresis, suggesting that the pore size is uniform and also the framework of the silica is composed of cylindrical channels without any intersecting disordered channels. However, compared with the pristine MCM-41 silica, the modified samples lack sharpness in the N_2 condensation step related to possible structural disordering. In addition, the pore size distribution (PSD) curves, obtained from the adsorption plot of the isotherm, show a sharp unimodal peak after modifications in the SBA-15 samples, whereas for the MCM-41 samples, the PSD curves broaden, showing materials with less well-ordered pore structures (Fig. 3, inset). Thus, the physisorption results indicate that under the present concentration of 3-APTS, the textural properties of SBA-15 are substantially maintained, whereas the MCM-41 samples show significant differences, in accordance with the XRD and TEM results.

Structural decay in mesoporous materials usually results from cleavage of the Si–O–Si bonds due to the presence of water molecules under drastic reaction conditions. In the present case, the wall thickness of pristine MCM-41 material is 0.8 nm, corresponding to only 3 $[SiO_4]^{4-}$ layers, whereas SBA-15 has an approximately five-fold greater wall thickness of 4.2 nm, which corresponds to around 10 $[SiO_4]^{4-}$ layers. Thus the increased wall thickness and thereby the increased stability of the silica framework in SBA-15 prepared under acidic conditions compared with the MCM-41 framework prepared under basic conditions explains the better stability of the SBA-15 solids compared with MCM-41 during modifications [18]. However, the postsynthesis modifications merit more attention; SBA-15 is not an extended form of MCM-41 with better stability and greater wall thickness. Generally, the calcined SBA-15, prepared at a synthesis temperature below 100 °C, has a large amount of micropores, whereas MCM-41 is devoid of such pore size discrepancies. Micropore formation is related to the penetration of hydrophilic EO chains into the silica framework, which on calcination provides heterogenity in pore structure [19]. However, in high-temperature SBA-15 synthesis, the degree of hydration around the EO blocks decreases, in turn causing a redistribution of the EO blocks to the core region of the micelles, leading to materials devoid of micropores. From *t*-plot analysis, we observed that the present SBA-15 samples are free from micropores, and that the micropore volume amounts to only ∼15% of the total pore volume of the sample. However, Kruk et al. suggested that the triblock copolymers are polydisperse mixtures with a range of molecular weights; that is, they contain appreciable amounts of diblock EO–PO units, as well as free PO units. These units, which do not participate in the cooperative assembly process between surfactant and oligomerized silicate, are believed to be involved in the creation of domains that constitute the complementary porosity of the SBA-15 samples [20]. Galarneau et al. observed a microporous corona surrounding the mesopores of the SBA-15 samples prepared at temperatures of 100–120 °C [21]. Thus even though *t*-plot analysis shows an absence of micropores in the SBA-15 samples, in reality the materials prepared at 100 °C have micropores. This discrepancy arises due to the sensitive assumptions adopted in the BET equation about the absence of micropores, as well as due to the lack of an appropriate reference isotherm [22]. Hence, for a better comparison over

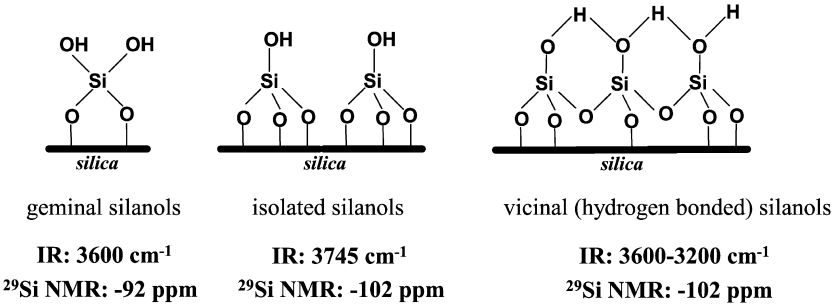

Scheme 1. Schematic representation of the silanol groups in silica surfaces and their respective IR and NMR values.

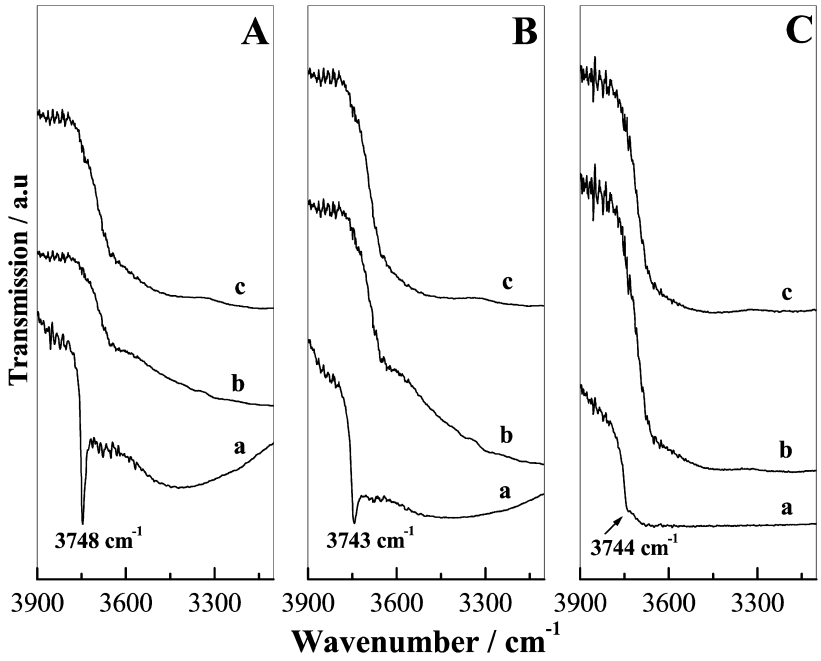

Fig. 4. OH vibrations of the IR spectra of (A) SBA-15, (B) MCM-41 and (C) silica gel, where (a) calcined sample, (b) aminopropyl modified sample and (c) vanadium-immobilized sample.

SBA-15 and MCM-41 mesoporous materials, SBA-15 samples prepared at 100 °C or higher are the optional candidates, because these procedures remove the micropores in the samples to a greater extent; otherwise, the materials might exhibit different adsorption properties due to the presence of micropores and mesopores.

3.2. Spectroscopic characterization

FTIR spectroscopy has been extensively used to study the surface properties of silica samples; in particular, the stretching vibrations of surface silanols (ν_{OH}) are very informative. The ν_{OH} stretching vibrations observed in the 3600–3200 cm^{-1} region are attributed to the hydrogen-bonded silanol groups, and the sharp bands at ~3740 cm^{-1} are attributed to the isolated surface silanol groups. Stretching vibrations of geminal silanols are also observed in the same region of isolated silanols; hence distinguishing these in the IR spectral patterns is very difficult [23–25]. But Takei et al. suggested that the shoulder band observed at around 3600 cm^{-1} relates to the presence of hydrogen-bonded and isolated geminal silanols [26] (Scheme 1). In the present analysis, after 3-APTS functionalization, complete disappearance of the isolated peak at 3740 cm^{-1} or a sharp decrease in its intensity with a peak shift to lower value is seen, demonstrating the role of surface silanols in modifications (Fig. 4). Moreover, it is also observed that the intensity of the hydrogen-bonded silanol groups in the 3600–3200 cm^{-1} decreases after 3-APTS functionalization. Generally, the free and geminal silanol sites are the active silanol sites participating in the condensation reactions with the silylating agents, whereas the hydrogen-bonded silanol groups do not actively participate due to the efficient hydrophilic networks formed among them [27]. However, the present results imply that the hydrogen-bonded silanol groups are also vulnerable in the reaction with aminopropyl groups. Removing surfactants from the pore channels of mesoporous materials and the attachment of aminopropyl groups over the silica surfaces were also examined by IR spectroscopy (Fig. 5). Calcination procedures are used for surfactant removal from Si-SBA-15 and Si-MCM-41 materials, with the understanding that complete removal of the surfactant groups can favor a uniform distribution of 3-APTS groups over the support surface. These proce-

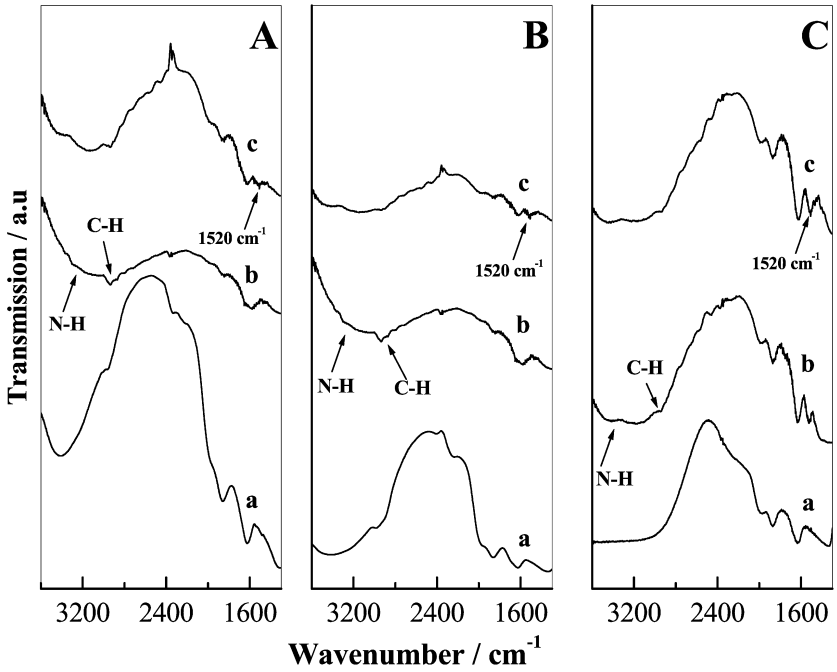

Fig. 5. FTIR spectra of (A) SBA-15, (B) MCM-41 and (C) silica gel samples, where (a) calcined sample, (b) aminopropyl modified sample and (c) vanadium-immobilized sample.

dures also prevent clogging of the aminopropyl moieties in the pore openings. The absence of strong absorption in the range of 2700–3000 cm^{-1} for the calcined SBA-15/MCM-41 sample clearly indicates the removal of surfactants, whereas the insertion of amino propyl groups is confirmed by the presence of N–H bending mode vibrations at 1520 cm^{-1} and at 3360 and 3290 cm^{-1}, corresponding to those of primary amines, and the C–H stretching vibration of methylene groups at 2960, 2850, and 1660 cm^{-1} [28–30]. These results corroborate the attachment of amino propyl groups on the solid supports. After vanadium immobilization, a shift in the amine peak to lower wave number is observed. These results explicitly indicate anchoring of the vanadyl cations on the tethered $–NH_2$ groups and also prove that the organo siloxane groups are linked to the silica surfaces through the formation of Si–O–Si bonds and not through any electrostatic interactions or hydrogen-bonding interactions between the amine groups and the Si–OH groups [14].

Further NMR experiments were done to evaluate anchoring of the silylating agents and to gain insight into how these silylation processes affect the structural properties of the support materials. The ^{13}C NMR spectra of 3-APTS-anchored mesoporous materials exhibit sharp, distinct resonance peaks at 9.2 ppm and 21.2 ppm for the carbon atom (C^1) adjacent to the amine moiety and to the central (C^2) carbon atom, whereas the carbon atom (C^3) bonded to the silicon shows a band at 42.8 ppm, with a shift in peak position to lower ppm values after the immobilization of vanadyl cations [14,28]. These results confirm that the aminopropyl groups are anchored to the support surface without any decomposition, as indicated by the IR evaluations. ^{29}Si NMR of propylamine-functionalized materials exhibits peaks at −110, 101, 92 (sh), −65 and −57 ppm, which are usually assigned to the Q^4 ($Si(OSi)_4$), Q^3 ($Si(OH)(OSi)_3$),

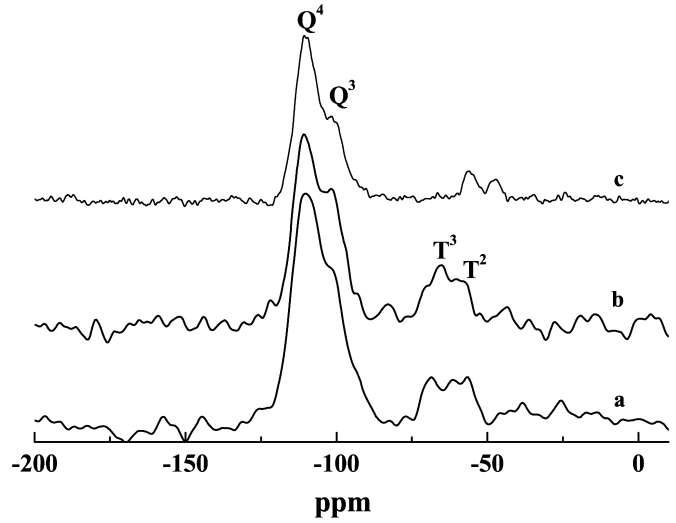

Fig. 6. ^{29}Si MAS NMR results of calcined samples, (a) SBA-15, (b) MCM-41 and (c) silica gel.

Q^2 ($Si(OH)_2(OSi)_2$), T^3 ($SiR(OSi)_3$), and T^2 ($Si(OH)R(OSi)_2$) sites, respectively (Fig. 6) [30,31]. For comparison, the spectra of calcined parent support samples are also given in Fig. 7. The broad resonance peaks of calcined samples from −90 to −110 ppm are typical for a range of Si–O–Si bond angles and the formation of more tetrahedral silicon environments. Compared with parent silica samples, amine-functionalized materials show decreases in Q^3 and Q^2 values with a corresponding increase in the percentage of Q^4 sites, demonstrating that the silylating agents effectively consume the geminal as well as the free silanol sites, as explained earlier. In general, the Q^3 sites are considered to be rich with isolated Si–OH groups, which may be free or hydrogen-bonded, whereas the Q^2 sites have

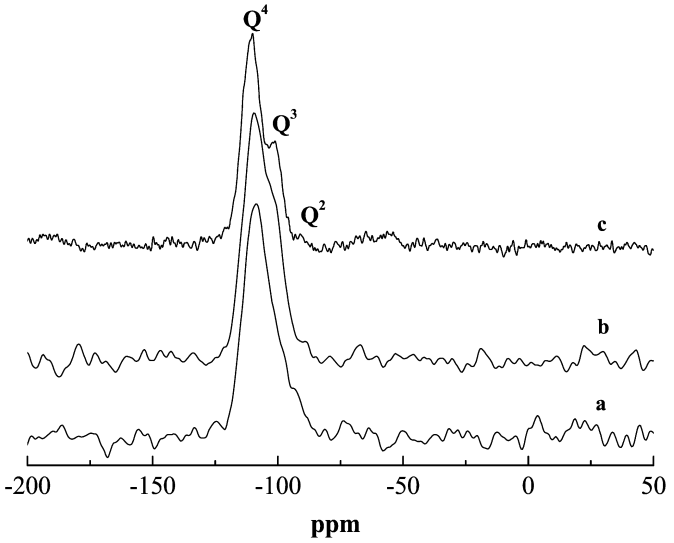

Fig. 7. ^{29}Si MAS NMR results of amino propyl modified silica samples, where (a) NH_2-SBA-15, (b) NH_2-MCM-41 and (c) NH_2-silica gel.

the geminal silanol sites [27]. A decrease in the Q^3 and Q^2 values after silylation over all of the support materials shows that these silanol groups are highly accessible to the silylating agents. The $(Q^3 + Q^2)/Q^4$ ratio indicates the presence of silanol groups residing on the support surface, and a lower $(Q^3 + Q^2)/Q^4$ value for amine-functionalized samples suggest that the material have few residual silanols, resulting in a siliceous pore wall structure with a greater degree of condensation and higher hydrothermal stability [31]. Among the support samples, the higher $(Q^3 + Q^2)/Q^4$ ratio in MCM-41 indicates that MCM-41 has more abundant silanol groups than SBA-15 and silica gel; these results nicely explain the higher amine loading over MCM-41 sample compared with the other two samples (Table 2). In addition, we see that after 3-APTS functionalization, the population of T^3 sites is concentrated more over MCM-41 than over SBA-15 and silica gel. Thus the differences in the T^2/T^3 results, summarized in Table 1, indicate that the population of silanol produced on the attached 3-APTS groups is more on silica gel, followed by SBA-15 and MCM-41, and suggests that the 3-APTS groups are more randomly distributed over the silica gel sample than the mesoporous materials [30]. Usually, the 3-APTS groups interact with one or two silanol groups of the support surface and become attached to the support as $SiC(SiO)(OH)_2$ or as $SiC(SiO)_2(OH)$, due to hydrolysis of the alkoxy groups. As mentioned earlier, the isolated and geminal silanol sites are the active silanols participating in the condensation reactions with the silylating agents, whereas the hydrogen-bonded silanol groups do not actively participate, due to the efficient hydrophilic networks formed among them. In the present synthesis procedures, before postsynthesis modification, we did not perform any water treatments over the support surface or any outgassing temperature treatments, to enhance the number of silanol groups and thereby increase the percentage of silylation. Thus the decreased T^2/T^3 ratio in NH_2-MCM-41 shows that more silanes are linked to each other here than in the pore channels of NH_2-SBA-15 and NH_2-silica gel surfaces.

Table 2
^{29}Si NMR data of pristine silica supports and amine-functionalized silica samples

Sample	$(Q^3 + Q^2)/Q^4$	T^2/T^3	$(T^2 + T^3)/(Q^2 + Q^3)$	$\sum T^n / \sum(T^n + Q^n)$
SBA-15	0.47	–		–
NH_2-SBA-15	0.24	1.28	0.75	13
MCM-41	0.59	–		–
NH_2-MCM-41	0.31	0.62	0.65	13.7
SG	0.33	–		–
NH_2-SG	0.18	2.5	0.85	11.8

Furthermore, the ratio of silicon from the organic groups to the total silicon present, $\{\sum T^n / \sum(T^n + Q^n)\}$, shows an increased value in MCM-41 (13.7) compared with SBA-15 (13.0) and silica gel (11.8). Hence, from the NMR interpretations, it can be concluded that more silanes are grafted on MCM-41 than on the large-pore SBA-15 and amorphous silica gel samples. Since steric factors do not affect grafting of silanes on the support surface, because the pore diameter of the two supports is significantly greater than the molecular size of silane, the decreased surface coverage over the SBA-15 surface may be due to the blockage of some organic groups near the pore mouth because of the complementary textual characteristics of SBA-15. Moreover, because the silylation procedures were performed under higher temperatures, it is likely that the flexible wall structure of the MCM-41 sample deteriorates to produce more silanol groups. These in situ formed silanol groups also may participate in the reaction with the organosilanols to enhance the percentage of 3-APTS groups compared with the hydrothermally stable SBA-15 sample. Proof of the formation of such silanols was not explored in this work, but the increased structural collapse as well as the increased 3-APTS loading of the NH_2-MCM-41 sample than the NH_2-SBA-15 sample inspired this suggestion. Thus, the more disordered structural features of the NH_2-MCM-41 material (from XRD/TEM/N_2 sorption measurements) may rely on a greater fixation of the Si–OR groups with the surface silanols, and the increased consumption of the silanol groups may enhance the structural disordering.

The UV–vis spectra of vanadium-immobilized aminopropyl samples are given in Fig. 8A. Even though the species anchored on the amino groups are V^{4+}, after all manipulations, the silica gel-supported vanadium complexes are almost yellow in color, whereas the mesoporous-supported vanadium catalysts are pale green-colored. From the color of the complexes prepared, it is possible that the oxidation state of vanadium residing over mesoporous NH_2-SBA-15/NH_2-MCM-41 and NH_2-silica gel samples are different. UV–vis spectra of all as-synthesized materials show three intense absorption bands in the UV region at 220, 280, and at 340 nm. The band observed at 220 nm is typical of siliceous materials but bands in the 250–350 nm range shows the presence of anchored vanadium. The absorption bands at 280 and 340 nm are assigned to the low-energy charge transfer bands between V=O electron transfer from $(\pi)t_2$ to $(d)e$ and $(\pi)t_1$ to $(d)e$ of tetrahedrally coordinated V^{5+} ions [12,14,32]. However, all samples lack the characteristic d–d transition of $(VO)^{2+}$ ions usually observed

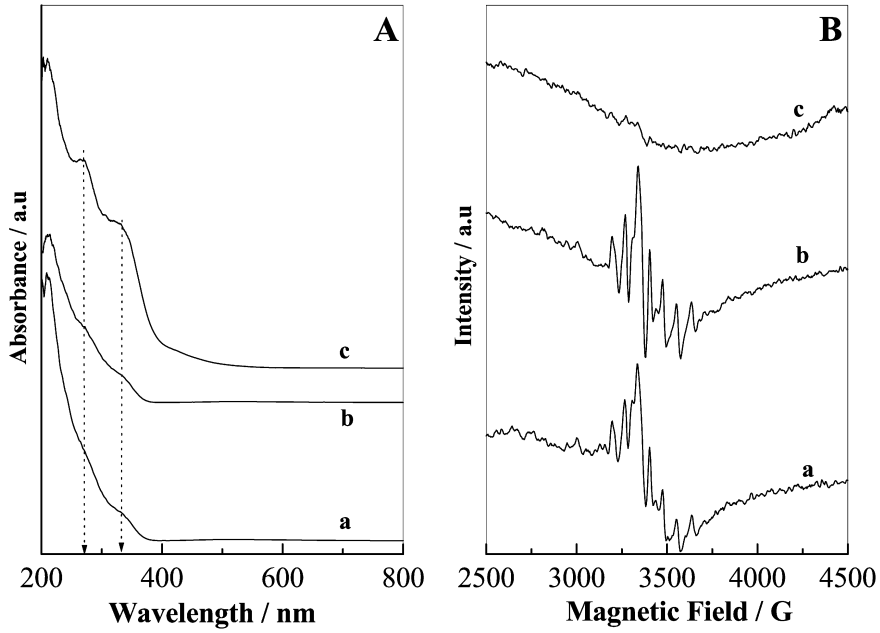

Fig. 8. (A) DR UV–vis spectra of vanadium-immobilized silica samples, where (a) VO–NH_2-SBA-15, (b) VO–NH_2-MCM-41, (c) VO–NH_2-silica gel and (B) EPR spectra of vanadium-immobilized silica samples, where (a) VO–NH_2-SBA-15, (b) VO–NH_2-MCM-41 and (c) VO–NH_2-silica gel.

in the visible region (600–800 nm). Hence, it is possible that the V^{4+} species may change its oxidation state from +4 to +5 during the drying process, and thus the concentration of V^{4+} groups on the support surfaces may be low. Moreover, because the *d–d* transitions are ∼10–30 times lower than the highly intense charge transfer (CT) transitions in the 250–400 nm range, a decreased intensity in the low-frequency region is also expected [12]. Among the three vanadium-immobilized samples, NH_2-silica gel-supported vanadium catalyst shows highly intense UV patterns. These results support the yellowish color of the VO–NH_2-silica gel sample for an increased amount of V^{5+} species. Because the surface coverage of aminopropyl groups was lowest over the silica gel sample, it is reasonable that the available amino groups are not able to stabilize the $(VO)^{2+}$ species. However, the increased percentage of amino groups, as well as pore confinement in mesoporous materials, may help to stabilize a part of the vanadium in the tetravalent state rather than over the silica gel surfaces and are further verified from the EPR spectral patterns.

The EPR spectra of vanadium-immobilized silica samples, recorded at room temperature, are given in Fig. 8B. The as-synthesized vanadium-containing mesoporous materials exhibit the anisotropic eight-line hyperfine patterns due to the interaction of the unpaired electron (V^{4+}, $3d^1$) with the nuclear spin of vanadium nuclei ($I = 7/2$). However, in accordance with UV–vis analysis, the silica gel-immobilized vanadium sample shows the absence of hyperfine splitting patterns, confirming that the entire vanadium anchored over silica gel is in a +5 oxidation state. The hyperfine splitting patterns obtained for the vanadium-containing mesoporous catalysts indicates that the $(VO)^{2+}$ ions are dispersed inside the pore channels of the mesoporous materials, and the observed *g* values and the hyperfine coupling constants are typical of $(VO)^{2+}$ ions with distorted pseudo-octahedral coordinations [12,33,34]. This interesting result suggest that the structural and textural features of mesoporous materials are more suitable for the entrapment of metal complexes in specific oxidation states than over the conventional silica gel surfaces. However, a combination of the UV–vis and EPR analysis shows that all of the vanadium-immobilized samples depicts the ligand-to-metal charge transfer (LMCT) transitions in the 200–400 nm range, typical of V^{5+} species, whereas the EPR patterns show the presence of V^{4+} in mesoporous samples. Because EPR is a sensitive characterization technique for detecting even ppm levels of vanadium, we speculate that the concentration of V^{4+} is significantly lower over the mesoporous materials. Raman analysis of all of the immobilized samples show a strong band at 1030 cm^{-1}, which is characteristic of isolated terminal $(NH_2)_3V{=}O$ groups being tetrahedrally coordinated (see supplementary information, Fig. 1S) [33]. According to Can Li, high-frequency bands correspond to shorter V–O bonds, and hence the bands >1000 cm^{-1} in the present case may correspond to the V=O species, which may arise from the isolated terminal metal sites, as mentioned previously [35]. Further, in agreement with the UV–vis and EPR results, the Raman spectra showed no band characteristic of crystalline V_2O_5, usually observed at around 995 cm^{-1}. The results of all of these characterization techniques indicate that vanadium exists as isolated sites in the immobilized catalyst systems.

3.3. Catalytic measurements

The catalytic activity of the heterogenized vanadyl complexes in the oxidation reaction of cyclohexane with aqueous hydrogen peroxide (30% H_2O_2) is given in Table 3. For comparison, this table also includes the activity over an isomorphously substituted vanadium-containing MCM-41 catalyst (V-MCM-41). From the table, it is apparent that the

Table 3
Oxidation of cyclohexane over vanadium-containing catalysts using H_2O_2 as an oxidant[a]

Catalyst	V[b] (%)	Cyane conversion (mol%)	Selectivity[c] (%)		K/A ratio[d]	TOF[e] (h^{-1}, 10^{-2})	Vanadium leaching[b] (%)
			Cy-ol (A)	Cy-one (K)			
V–NH_2-SBA-15	0.92	21	58	42	0.72	9	11
V–NH_2-MCM-41	0.95	19	62	38	0.61	8	13
V–NH_2-SG	0.93	18	54	46	0.85	8	31
V–MCM-41	0.98	15	52	48	0.92	6	22

[a] Reaction conditions: T (°C) = 80; cyclohexane:oxidant (mol/mol) = 1; catalyst weight = ~10% of cyclohexane; solvent, CH_3CN (ml) = 5; time (h) = 12.
[b] Vanadium content (wt%) determined by ICP-OES analysis.
[c] Cy-ol = cyclohexanol; Cy-one = cyclohexanone.
[d] K/A = ketone by alcohol ratio.
[e] Turnover frequency (TOF) = moles of cyclohexane converted/(mole of vanadium per hour).

vanadium-immobilized mesoporous catalysts have greater activity and higher turnover frequency (TOF) than the framework-substituted V-MCM-41 catalyst. The increased catalytic activity of the immobilized vanadium catalysts compared with the V-MCM-41 catalyst may arise from active site isolation, that is, attachment of catalyst to a support in such a way that the catalytic sites no longer interact with each other. Thus effective site isolation, better coordination of the metal with the ligands, and tight attachment of ligands to the support may favor the higher catalytic activity of the immobilized vanadium catalysts compared with the V-MCM-41 catalyst [14,36]. Furthermore, all of the vanadium-immobilized aminopropyl catalysts show almost similar conversion and TOF values. This result suggests the presence of similar vanadium structures over all of the immobilized catalysts, and hence the coordination of vanadium is presumed to be similar over all support systems.

The slightly improved catalytic performance of the vanadium-immobilized mesoporous catalysts compared with the VO–NH_2-SG catalyst can be explained by the pore confinement effect, in which the substrate-favorable interactions with both the pore walls as well as the catalyst molecule enhance the conversion rate over the silica gel surfaces. In addition, the vanadium-immobilized NH_2-SBA-15 sample shows slightly higher activity than the NH_2-MCM-41 sample. We attribute this improved catalytic activity to the complementary pore characteristics of the SBA-15 materials compared with the one-dimensional channel-oriented MCM-41 mesoporous support. We are working on exploiting the catalytic activity of the SBA-15 materials synthesized at lower temperatures and thereby provide more evidence on the role of micropores or small mesopores in enhancing activity and selectivity during catalysis. Moreover, the present results raise the reasonable question as to whether V^{4+}–O–O$^{\cdot}$ or V^{5+}–O–O$^{\cdot}$ species are the active vanadium sites for the present reaction. Because the vanadium-immobilized SBA-15 sample gives the maximum conversion results, the EPR spectrum of this sample is taken after its treatment with aqueous H_2O_2. The addition of H_2O_2 immediately changed the color of the catalyst from pale green to yellowish, and the EPR analysis shows the absence of eight-line hyperfine splitting patterns. Thus H_2O_2 treatment changed the oxidation state of heterogenized vanadium from its +4 state to the EPR silent +5 state, and hence it is possible that the active vanadium peroxo complex species may be the V^{5+}–O–O$^{\cdot}$ species [12,37].

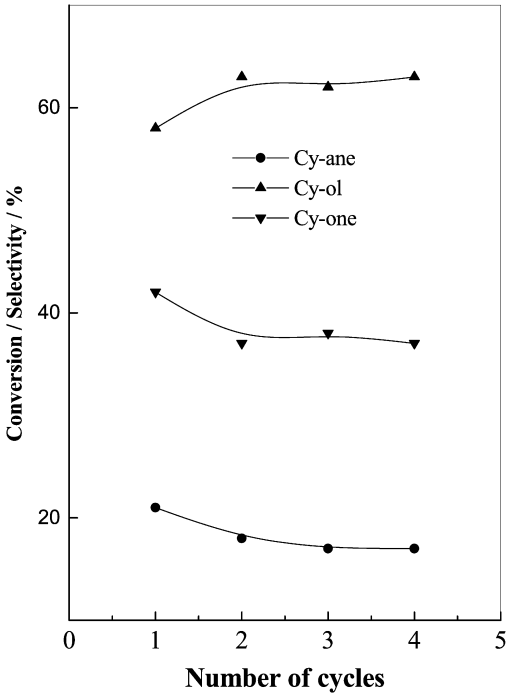

Fig. 9. Recycling studies performed over VO–NH_2-SBA-15 catalyst.

3.4. Recycle studies

To assess whether the activity of the heterogenized vanadium catalysts arises from stable mesoporous materials, metal leaching studies were also performed, because they provide better structure-activity correlations. ICP-OES analysis was used to determine the percentage of vanadium leached out into the liquid mixture during reactions. In addition, XPS analysis of the N1s is also carried out to verify whether the amine groups had undergone some sort of oxidation reaction in the presence of oxidants (see supplementary information, Fig. 2S). The results show an almost similar peak position for the N1s (of –NH_2 species) for the fresh and spent catalysts, and the reaction products confirm the absence of oxidation of the amine groups in 3-APTS (from gas chromatography analysis). However, ICP analysis showed that for the heterogenized vanadium catalysts, the extent of leaching decreases in the following order: V–NH_2-SG > V-MCM-41 > V–NH_2-MCM-41 > V–NH_2-SBA-15 (Table 3). Thus, the percentage of vanadium leaching

in V-MCM-41 and VO–NH_2-silica gel samples is ∼2–3 times higher than in vanadium-immobilized NH_2-SBA-15 and NH_2-MCM-41 catalysts. The increased leaching of vanadium from the VO–NH_2-SG sample is related to the weak anchoring of the 3-APTS groups over the silica gel surface (increased T^2 sites from NMR results) and the further breakage of –Si–O–Si^*– (Si^* related to the silicon of organosilane) bonds in the presence of aqueous oxidant. However, the decreased heterogenity of the V-MCM-41 catalysts is related to the high-temperature calcination process for template removal and also to the structural collapse of the mesoporous material in the presence of aqueous oxidants [12,14]. In addition, several recycling runs were performed over the VO–NH_2-SBA-15 catalyst (Fig. 9); results showed that the conversion decreases slightly during the first recycle (second run) and the conversion and product selectivity remain more or less the same thereafter. This leveling-off of conversion and selectivity during subsequent cycles (up to the fourth run) shows the existence of tightly held, isolated vanadium sites, because if the metal were leached out, then the conversion as well as selectivity should vary during subsequent recycling. These results demonstrate the novelty of heterogenizing metal complexes in mesoporous materials through organo-tethered groups, with the enhanced activity and better stability of the mesoporous hosts attributed to the active metal site isolation, a more hydrophobic environment, and the spatial restrictions imparted by the concave silica surface in SBA-15 and MCM-41 compared with the convex silica surface of the silica gel sample [38].

4. Conclusion

The present study has provided comprehensive data on the structural and textural changes over mesoporous supports with p6mm symmetry during aminopropyl functionalization and a comparison with amorphous silica gel samples. Our findings suggest that the pore geometry and textural features of the support surface exert considerable influence on the nature of the fixation of the silylating groups and subsequent metal complexation processes, which in turn influence the catalytic activity and stability of the final materials. Vanadium-immobilized NH_2-SBA-15 and NH_2-MCM-41 catalysts show maximum conversion and better stability than the NH_2-silica gel-immobilized vanadium sample and a V-MCM-41 sample. The better activity and stability obtained over amine-functionalized mesoporous vanadium catalysts are attributed to the better site isolation, more hydrophobic environment, and increased pore confinement effect compared with the V-MCM-41 and NH_2-silica gel-immobilized vanadium catalysts. The present synthesis strategies open new avenues to effectively introduce active redox sites in mesoporous silica surfaces through organo-tethered groups.

Acknowledgments

The authors thank the reviewers for constructive suggestions and Dr. D. Srinivas, Dr. N.R. Shiju, Mr. R.K. Jha, Mrs. Renu Parischa, and Mrs. Kavitha for the characterization results and useful discussions. S.S. thanks CSIR, India, for a senior research fellowship and acknowledges the CSIR task force project (scheme under "Catalysts and Catalysis"/ P23-CMM 0005-B) for financial assistance.

Supplementary information

The online version, of this article contains additional supplementary information at doi: 10.1016/j.jcat.2006.08.002.

References

[1] C.T. Kresge, M.E. Leonowicz, W.J. Roth, J.C. Vartuli, J.S. Beck, Nature 359 (1992) 710.
[2] D. Zhao, Q. Huo, J. Feng, B.F. Chmelka, G.D. Stucky, J. Am. Chem. Soc. 120 (1998) 6024.
[3] A. Sayari, Chem. Mater. 8 (1996) 1840 and references therein.
[4] A. Corma, Chem. Rev. 97 (1997) 2373.
[5] J.Y. Wing, C.P. Mehnert, M.S. Wong, Angew. Chem. Int. Ed. Engl. 38 (1999) 56.
[6] A. Stein, B.J. Melde, R.C. Schroden, Adv. Mater. 12 (2000) 1403.
[7] A. Taguchi, F. Schuth, Microporous Mesoporous Mater. 77 (2004) 1.
[8] B. Marler, U. Oberhagemann, S. Vortmann, H. Gies, Microporous Mater. 6 (1996) 375.
[9] D. Brunel, Microporous Mesoporous Mater. 27 (1999) 329.
[10] D.E. De Vos, B.F. Sels, P.A. Jacobs, Adv. Catal. 46 (2001) 1.
[11] T. Joseph, S.S. Deshpande, S.B. Halligudi, A. Vinu, S. Ernst, M. Hartmann, J. Mol. Catal. A Chem. 206 (2003) 13.
[12] C.-H. Lee, T.-S. Lin, C.-Y. Mou, J. Phys. Chem. B 107 (2003) 2543.
[13] R.A. Sheldon, M. Wallau, I.W.C.E. Arends, U. Schuchardt, Acc. Chem. Res. 31 (1998) 448.
[14] S. Shylesh, A.P. Singh, J. Catal. 228 (2004) 333.
[15] A.S.M. Chong, X.S. Zhao, J. Phys. Chem. B 107 (2003) 12650.
[16] D. Zhao, J. Feng, Q. Huo, N. Melosh, G.H. Fredrickson, B.F. Chmelka, G.D. Stucky, Science 279 (1998) 548.
[17] J.A. Melero, G.D. Stucky, R. Grieken, G. Morales, J. Mater. Chem. 12 (2002) 1664.
[18] K. Cassiers, T. Linssen, M. Mathieu, M. Benjelloun, K. Schrijnemakers, P. Van der Voort, P. Cool, E.F. Vansant, Chem. Mater. 14 (2002) 2317.
[19] M.S. Morey, S. O'Brien, S. Schwarz, G.D. Stucky, Chem. Mater. 12 (2000) 898.
[20] M. Kruk, M. Jaroniec, C.H. Ko, R. Ryoo, Chem. Mater. 12 (2000) 1961.
[21] A. Galarneau, H. Cambon, T. Martin, L.-C. de Menorval, D. Brunel, F.D. Renzo, F. Fajula, Stud. Surf. Sci. Catal. 141 (2002) 395.
[22] A. Galarneau, H. Cambon, F.D. Renzo, F. Fajula, Langmuir 17 (2001) 8328.
[23] T. Ishikawa, M. Matsuda, A. Yasukawa, K. Kandori, S. Inagaki, T. Fukushima, S. Kondo, J. Chem. Soc. Faraday Trans. 92 (1996) 1985.
[24] A. Jentys, N.H. Pham, H. Vinek, J. Chem. Soc. Faraday Trans. 92 (1996) 3287.
[25] T.W. Dijkstra, R. Duchateau, R.A. van Santen, A. Meetsma, G.P.A. Yap, J. Am. Chem. Soc. 124 (2002) 9856.
[26] T. Takei, K. Kato, A. Meguro, M. Chikazawa, Colloids Surf. A 150 (1999) 77.
[27] X.S. Zhao, G.Q. Lu, J. Phys. Chem. B 102 (1998) 1556.
[28] X. Wang, Y.-H. Tseng, J.C.C. Chan, S. Cheng, J. Catal. 233 (2005) 266.
[29] A.B. Bourlinos, Th. Karakoatas, D. Petridis, J. Phys. Chem. B 107 (2003) 920.
[30] H. Yoshitake, T. Yokoi, T. Tatsumi, Chem. Mater. 14 (2002) 4603.
[31] W.H. Zhang, X.-B. Lu, J.-H. Xiu, Z.-L. Hua, L.-X. Zhang, M. Robertson, J.-L. Shi, D.-S. Yan, J.D. Holmes, Adv. Funct. Mater. 14 (2004).
[32] (a) M. Chatterjee, T. Iwasaki, H. Hayashi, Y. Onodera, T. Ebina, T. Nagase, Chem. Mater. 11 (1999) 1368;
Z. Luan, J. Xu, H. He, J. Klinowski, L. Kevan, J. Phys. Chem. 100 (1996) 19595.

[33] M. Mathieu, P. Vander Voort, B.M. Weckhuysen, R.R. Rao, G. Catana, R.A. Schoonheydt, E.F. Vansant, J. Phys. Chem. B 105 (2001) 3393.
[34] P. Selvam, S.E. Dapurkar, J. Catal. 229 (2005) 64.
[35] G. Xiong, C. Li, H. Li, Q. Xin, Z. Feng, Chem. Commun. (2000) 677.
[36] J.M. Thomas, T. Maschmayer, B.F.G. Johnson, D.S. Shephard, J. Mol. Catal. A Chem. 141 (1999) 139.
[37] H. Mimoun, L. Saussine, E. Daire, M. Postel, J. Fischer, R. Weiss, J. Am. Chem. Soc. 105 (1983) 3101.
[38] J.M. Thomas, R. Raja, Stud. Surf. Sci. Catal. 148 (2004) 163.